RSC Advances

ROYAL SOCIETY OF CHEMISTRY

www.rsc.org/advances

Low Band Gap Disk-shaped Donors for Solution-Processed Organic Solar Cells

Keisuke Takemoto and Mutsumi Kimura*

Division of Chemistry and Materials, Faculty of Textile Science and Technology, Shinshu University, Ueda 386-8567, Japan

Corresponding Author: Prof. Dr. M. Kimura

Mail address: *Division of Chemistry and Materials, Faculty of Textile Science and Technology, Shinshu University, Ueda386-8567, Japan*

TEL & FAX: +81-268-21-5499

E-mail: mkimura@shinshu-u.ac.jp

Type: Full Article

Table of contents: Color graphic

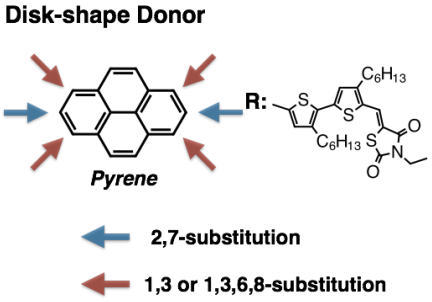

TEXT: Performance of pyrene-cored donors in BHJ solar cells is enhanced by introduction of rhodanine due to expansion of light-harvesting area.

Abstract:

Disk-shaped donors **1-4** composed of a pyrene core, dithiophene linkers and rhodanine terminates were synthesized and their optical and electrochemical properties were investigated. The introduction of rhodanine terminal units into the pyrene-cored donors could effectively broaden the absorption spectrum and improve the molar absorption coefficient. The positions of thiophene oligomer in the pyrene core affected to their optical and electrochemical properties as well as the molecular ordering and carrier transport properties in solid state. The energy levels of these molecules are suitable for the donor components in bulk heterojunction solar cells with fullerene derivatives. A **4**/$PC_{71}BM$ cell achieved an overall power conversion efficiency of 3.7% with a

short-current density of 8.4mA/cm^2, open-circuit voltage of 1.09V, and fill factor of 41% under one sun condition.

Introduction

Organic photovoltaic devices (OPVs) based on thin films of organic semiconductors have been intensely investigated as a promising alternative of conventional silicon-based solar cells because of their potential for low-cost and scalable manufacturing through solution-based printable technologies on flexible substrates.[1,2] The performance of OPVs has been greatly improved by using bulk heterojunction (BHJ) architecture, which is an interpenetrating network with a large donor-acceptor interfacial area organized through a spontaneous phase-separation of donor and acceptor materials.[3,4] Controlling BHJ structure in the active layers allows a high interfacial area that optimizes the exciton dissociation as well as the efficient transport of generated charge carriers to the respective electrodes.[5]

A wide variety of π-conjugated oligomers and polymers have been designed and synthesized as light-harvesting donor materials for the solution-processed BHJ solar cells.[6-10] Compared to π-conjugated polymers, discrete and well-defined π-conjugated oligomers are advantageous because the nanostructures in the active layers of the BHJ solar cells can be precisely controlled.[11-20] Moreover, the optoelectronic properties of π-conjugated oligomers such as optical properties, charge carrier mobility, and energy levels can be tuned systematically by chemical functionalizations. To date, an overall power conversion efficiency (PCE) of around 8% has been achieved in solution-processed BHJ solar cells by blending active layers of low band gap donor

oligomers with the fullerene derivative [6,6]-phenyl-C71-butylic acid methyl ester ($PC_{71}BM$).[21] Recently, we reported on the performance of BHJ solar cells containing self-organized stacks of pyrene-cored donors.[22] Pyrene has been used as a molecular component of organic semiconductors for organic electronics.[23-25] The modification by varying the substitution at different positions of the pyrene ring allows the tuning of optical and electronic properties, and the molecular shape of pyrene derivatives affects the molecular packing in the solid state. Pyrene-cored donors with linear oligothiophenes were organized into one-dimensional stacks through intermolecular π-π interaction, and the π-π overlap within the stacks provided an efficient transport pathway for charge or energy.[22] However, PCEs of pyrene-cored donors with $PC_{71}BM$ was less than 3% due to the limitation of light-harvesting area of active layers.

The introduction of acceptor units in the donors gives strong absorption at a long wavelength owing to intramolecular charge transfer.[26,27] To expand the light-harvesting area of pyrene-cored donors for the solution-processed BHJ solar cells, we designed four pyrene-cored donors **1-4** terminated with rhodanine acceptor units, in which the pyrene core and rhodanine terminal units were linked with alkyl-substituted dithiophene π-conjugated linkers to form a conjugated backbone structure with strong charge transfer and broad absorption. A PCE of 3.7% with an open-circuit voltage (V_{oc}) above 1.0 V was achieved for solution-processed BHJ solar cells using **4** with $PC_{71}BM$ under one-sun condition.

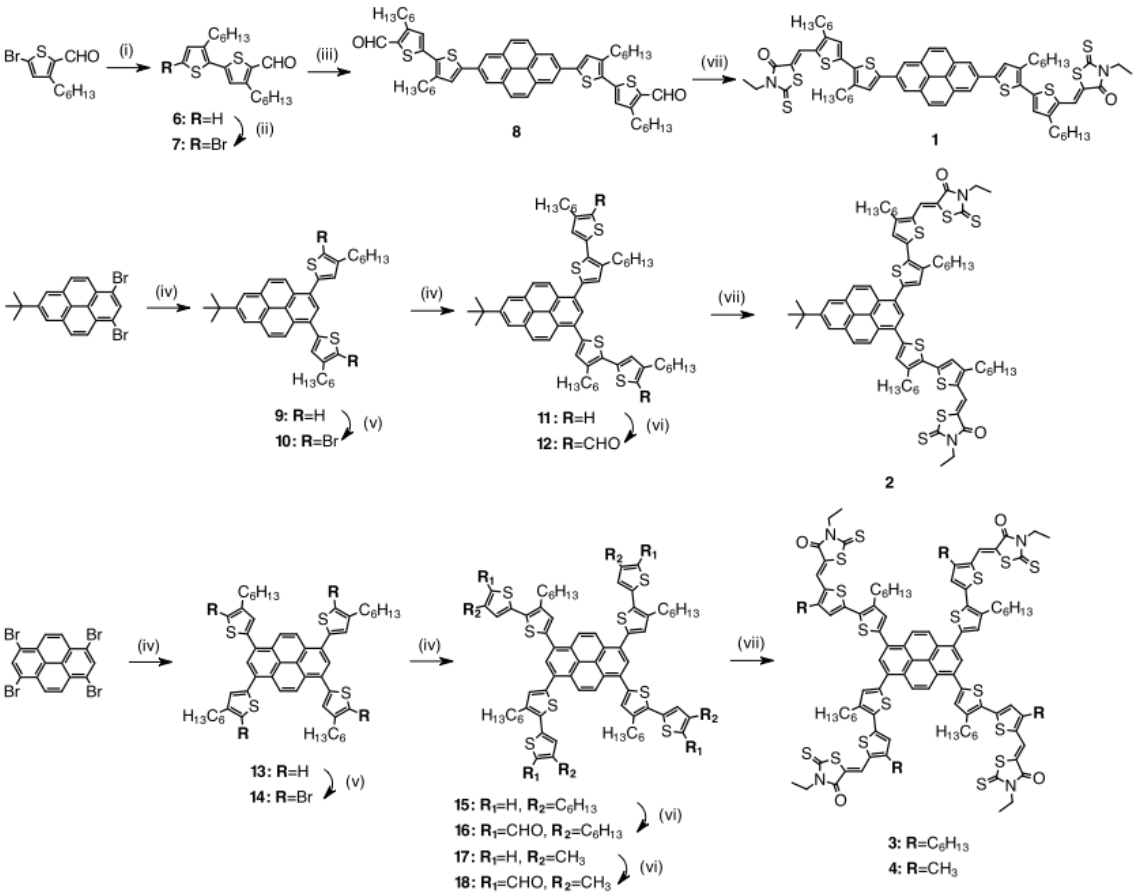

Scheme 1. Synthesis of pyrene-cored donors **1-4**. Reaction conditions: (i) 3-hexylthiophene-2-boronic acid pinacol ester, THF/ K_2CO_3; (ii) NBS, $CHCl_3$/ AcOH; (iii) 2,7-Bis(4,4,5,5-tetramethyl-1,3,2-dioxaborolan-2-yl)pyrene, toluene/ ethanol/ K_2CO_3; (iv) 4-hexylthiophene-2-boronic acid pinacol ester or 4-methylthiophene-2-boronic acid pinacol ester, toluene/ ethanol/ K_2CO_3; (v) NBS, $CHCl_3$; (vi) $POCl_3$, 1,2-dichloroethane/ DMF; (vii) 3-ethylrhodanine, piperizine/ $CHCl_3$.

Results and Discussion

Four pyrene-cored donors **1-4** based on he different substitution patterns of pyrene were synthesized through stepwise reactions from di- or tetrasubstituted pyrenes (Scheme 1). Linear 2,7-disubstituted donor **1** was synthesized by Suzuki-Miyaura coupling reaction with dithiophene derivative **6** and 2,7-bis(4,4,5,5-tetramethyl-1,3,2-dioxaborolan-2-yl)pyrene and the following Knoevenagel reaction with

3-ethylrhodanine. The other three donors **2-4** were prepared from 1,3-dibromo-7-*tert*-butylpyrene or 1,3,6,8-tetrabromopyrene. After the formylation of terminal positions through a Vilsmeir reaction, 3-ethylrhodanine units were introduced at the aldehydes to give **2-4**. The rhodanine units have been used as an electron-deficient group in the low band gap organic semiconductors for BHJ solar cells.[21,22,28] The purity of the targeted compounds **1-4** for device fabrication was guaranteed by repeated column purifications, and checked by analytical HPLC and MALDI-TOF-Ms. All pyrene-cored donors exhibit a good solubility in organic solvents such as $CHCl_3$, toluene and chlorobenzene. The solubility of **1-4** in $CHCl_3$ or chlorobenzene is above 20mg/ml at 20^{o}C. Uniform thin films were formed by spin-coating of donor solutions on quartz substrates. Pyrene-cored donors with good solubility and film forming property are a prerequisite for solution-processed BHJ solar cells.

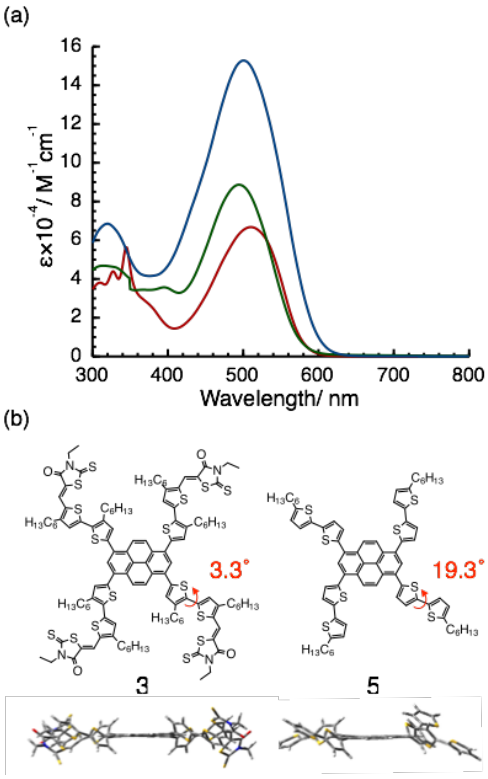

Figure 1. (a) UV-Vis absorption spectra of **1-3** in chloroform. (b) Optimized molecular geometries of **3** and **5** by DFT calculation with B3LYP 6-31G* level.

Table 1. Absorption, electrochemical, thermal, and hole-mobility data of **1-4**.

	Solution		Film	E_{ox}[c]	m.p.[d]	μ_h[e]
	λ_{max} /nm[a]	$\varepsilon\times10^{-4}$ /M^{-1} cm^{-1}	λ_{max} / nm[b]	/ V *vs.* Fc/Fc^+	/ °C	/ cm^2 V^{-1} s^{-1}
1	327, 345, 510	4.4, 5.6, 6.7	349, 534	0.71	286	1×10^{-4}
2	314, 395, 494	4.7, 3.5, 8.9	321, 502	0.76	160	1×10^{-4}
3	320, 501	6.9, 15.3	331, 526	0.56	181	1×10^{-5}
4	321, 502	6.0, 14.5	334, 530	0.57	234	6×10^{-5}

[a] Maximum of the absorption in $CHCl_3$. [b] Deposited onto quartz substrate by spin-coating technique from $CHCl_3$ solution. [c] Measured in degassed $CHCl_2$ containing 0.1M $TBAPF_6$ at 295K, scan rate =100mV/s. [d] Determined by DSC operated at a scanning rate of 10°C/min. [e] Determined from SCLC method using hole-only device with **1-4** films prepared by spin-coating from $CHCl_3$ or chlorobenzene solution.

Figure 1a shows the UV-Vis spectra of **1-3** in $CHCl_3$, and the absorption maxima (λ_{max}) and molar absorption coefficients (ε) of **1-4** are collected in Table 1. Compound **3** decorated with four 3-ethylrhodanine-terminated dithiophenes exhibits an absorption peak at 501 nm with ε value of 1.5 x $10^5 M^{-1}$ cm^{-1}. The absorption maxima of **3** exhibits a 48 nm red-shift compared to the pyrene-cored donor lacking rhodanine terminal units **5** (λ_{max}=453nm), and the ε value of **3** was almost three times higher than that of **5**.[22] The introduction of electron accepting terminal units into the pyrene-cored donors could effectively broaden the absorption spectrum and improve the ε value. Furthermore, the position and number of side chains also affected the λ_{max} and ε values. The band gap of organic semiconductors can be compressed by applying the intramolecular charge transfer between electron-rich donors and electron-deficient acceptors.[26,27,29] The interaction between donor and acceptor units gives rise to an increased double bond character between these two units. The dihedral angle between thiophene units in the optimized structure of **3** (3^o) is smaller than that in **5** (19^o), suggesting that the increase of double bond character between two thiophene units is caused by the introduction of rhodanine terminates (Figure 1b). Broad absorption ranges and high ε values of rhodanine-terminated donors are anticipated to efficient capturing of photon energy in solar cell devices.

The energy gap between the highest occupied molecular orbital (HOMO) of the donor and the lowest unoccupied molecular orbital (LUMO) of the acceptor correlate with the potential output of the devices. The HOMO energy levels of **1-4** were determined by cyclic voltammetry in combination with differential pulse voltammetry

(DPV) in dry CH_2Cl_2 containing 0.1M tetrabutylammonium hexafluorophosphate ($TBAPF_6$) as a supporting electrolyte (Table 1). The cyclic voltammograms of **1-4** reveal reversible one-electron oxidation at 0.71, 0.76, 0.56 and 0.57V *vs.* ferrocene/ferrocenium redox couple (Fc/Fc^+). The HOMO energy levels of **1-4** were calibrated from the oxidation potentials determined from DPV (Table 1).[30]

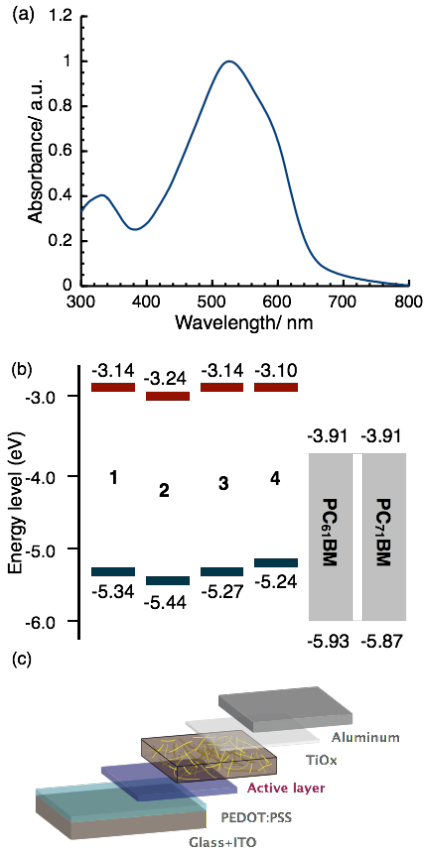

Figure 2. (a) Absorption spectra of spin-coated thin film of **3**. (b) Energy diagrams of **1-4**, $PC_{61}BM$, and $PC_{71}BM$. (c) Structure of BHJ solar cells

The spin-coated film of **3** shows a broader absorption from 300-670nm and a red-shifted λ_{max} at 526nm with a vibronic shoulder peak at 600nm (Figure 2a, Table 1). These spectral changes indicate π-π packing between the molecule backbones in the solid state.[31,32] The LUMO energy levels for **1-4** were estimated from the HOMO

energy levels, and the optical energy gaps ($E_{0\text{-}0}$) determined from the onset of absorption bands of the thin films. Figure 2b shows the energy band diagrams of **1-4** in relation to the relative energy levels of fullerene derivatives. The HOMO level of rhodanine-terminated **3** is similar to that of **5**, whereas the LUMO level of **3** was significantly stabilized through the electron accepting effect of rhodanine terminates. The LUMO energy levels of all pyrene-cored donors are still higher than those of [6,6]-phenyl-C61-butylic acid methyl ester ($PC_{61}BM$) and $PC_{71}BM$, revealing a sufficient driving force for electron transfer after photoexcitation.[1,2] Thus, the pyrene-cored donors **1-4** are expected to be a suitable candidate for the donor materials in BHJ solar cells with $PC_{61}BM$ or $PC_{71}BM$.

The thermal properties of **1-4** were characterized using themogravimetric analysis (TGA) and differential scanning calorimetry (DSC) (Figure S3). TGA analyses showed that all pyrene-cored donors **1-4** exhibit a good thermal stability with decomposition temperatures of above 350^{o}C under an N_2 atmosphere. The DSC analyses of **1-4** revealed one endothermic peak, corresponding to the melting point (Table 1). The melting points of organic molecules are determined by factors including molecular symmetry, electric dipoles, and interaction energies.[33] The melting point of **4** is higher than that of **3**, revealing the increase of intermolecular interaction energy by shortening the alkyl chains of the outer thiophene units in the peripheral substituents. The structural ordering of **1-4** was investigated by powdered XRD analyses (Figure S4). The reflection patterns of **1** showed several reflection peaks at 2θ=2-30^{o}, indicating a high degree of crystallinity. In contrast, the XRD patterns of **2-4** did not provide any peaks at 2θ=2-15^{o}.

The films of **2** and **4** exhibited a sharp reflection peak at 0.37nm due to the stacking distance between rigid aromatic segments, suggesting the presence of long-range periodicity in stacks.

The hole mobilities of **1-4** in the thin films were evaluated by space charge limited current (SCLC) method (Table 1).[34-38] The hole mobility of **3** was ten times less than those of **1** and **2**, presumably due to the low degree of crystallinity of **3** as described in the XRD analyses. On the other hand, **4** showed a six times higher mobility compared to **3**, implying that the stacking provides a transport pathway for holes in the solid state.

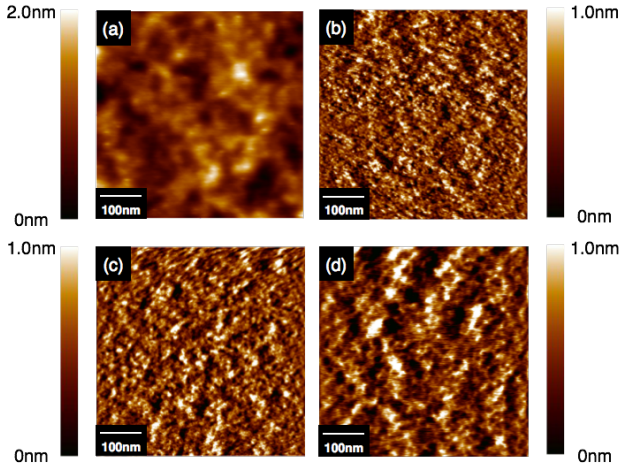

Figure 3. Tapping-mode AFM height images of **1-4**/$PC_{61}BM$ blended film.

Control of the phase-segregation structure in the blended active layers is an important factor in enhancing the PCE of BHJ solar cells. The surface morphology of blended films was examined by tapping mode atomic force microscopy (AFM) (Figure 3).[11,13,15] The blended films were prepared by the spin coating from the chloroform solution of **1-4** and $PC_{61}BM$ on quartz substrates. The blended film of **1**/$PC_{61}BM$

showed large-sized domains with an average size above 50nm. The topography image of **2**/$PC_{61}BM$ comprises small domains less than 20 nm wide with a surface roughness (rms) of 0.27nm. The blended films of **3** or **4** with $PC_{61}BM$ are also smooth with an rms less than 1 nm. The AFM images indicates that **2-4** have a good miscibility with $PC_{61}BM$ in the blended films and the spontaneous phase-segregation process in the mixed layer can form a bicontinuous network structure, which acts as percolation channels for the efficient carrier collection within the active layer of BHJ solar cells.[3,4]

Table 2. Summary of device parameters of BHJ solar cells based on mixed active layers of **1-4** and P3HT/ PCBMs.

Active layer (weight ratio w/w)	thickness /nm	V_{oc} / V	J_{sc} /mA cm^{-2}	*FF*	PCE / %
1/ $PC_{61}BM$ (1:2)	65	1.04	3.21	0.33	1.1
2/ $PC_{61}BM$ (1:4)	70	1.15	2.87	0.29	1.0
3/ $PC_{61}BM$ (1:4)	70	1.11	5.53	0.38	2.3
4/ $PC_{61}BM$ (1:2)	70	1.10	5.50	0.36	2.1
4/ $PC_{61}BM$ (1:3)	70	1.13	6.30	0.39	2.8
4/ $PC_{61}BM$ (1:4)	70	1.10	5.97	0.39	2.5
4/ $PC_{71}BM$ (1:3)	70	1.08	8.42	0.41	3.7
P3HT/ $PC_{61}BM$ (2:1)	90	0.65	8.38	0.67	3.7

BHJ solar cells were fabricated using **1-4** as the electron donor and $PC_{61}BM$ or $PC_{71}BM$ as the electron acceptor with tin-doped indium oxide (ITO)/ poly(3,4-ethylenedioxythiophene):polystyrene sulfonate (PEDOT:PSS)/ active layer/TiO_x/aluminium device structure using a solution process (Figure 2c). The cleaned

ITO was modified by spin-coating of PEDOT:PSS as a hole-extraction/electron-blocking layer with a 40nm thickness. The active layer was deposited from a chloroform solution onto the PEDOT: PSS modified ITO anodes in an argon-filled grove box, and the thickness was typically 60-70nm. The TiO_x layer was used as an electron-collection/hole-blocking layer in the BHJ solar cells. Finally, an aluminum cathode was deposited through a shadow mask by thermal evaporation under vacuum. The performances for all devices under AM 1.5G illumination at an intensity of 100 $mWcm^{-2}$ are summarized in Table 2. The cell performance of a poly(3-hexyl)thiophene (P3HT)/$PC_{61}BM$ device is provided as a benchmark. The effect of the different composition of **4**/ $PC_{61}BM$ was investigated (Table 2). The weight ratio of 1:2 w/w of **4**/$PC_{61}BM$ showed a PCE of 2.1% with a V_{oc} of 1.10V, short-current density (J_{sc}) of 5.50mA/ cm^2 and fill factor (*FF*) of 36%. When the composition ratio of **4**/$PC_{61}BM$ was changed to 1:3 w/w, the PCE increased to 2.8%. Further increase of composition ratio show a drop in the PCE value.

The PCE value was in the order of **1** = **2** < **3** < **4** cells in the optimized composition ratios of donor/$PC_{61}BM$ (Figure S6, Table S1). The PCE values strongly depended on the structure of pyrene-cored donors. The replacement of hexyl chains in **3** with methyl groups in **4** resulted in a higher PCE of 2.8 %. This higher PCE for **4** corresponds to higher J_{sc} and *FF* values relative to **3**, which is believed to be due to its better hole mobility in stacking. The BHJ solar cells based on **2-4** exhibited high V_{oc} values of > 1.0 V. The rhodanine-terminated donors based on benzo[1,2-*b*:4,5-*b'*]dithiophene unit also exhibited high V_{oc} values above 0.9V in the solution processes BHJ solar cells as

reported by Zhou et el.[20, 21] The origin of high V_{oc} values was analyzed by fitting the dark current density-voltage curve using the Shockley diode model modified for organic solar cells.[39-41] The J_{SO} values obtained from the Shockley equation have been used as an index for the strength difference of intermolecular interactions of donors with $PC_{61}BM$ in the active layer. The J_{SO} value for the **4**/$PC_{61}BM$ cell (4.80×10^{-3} mA/cm^2) was much smaller than that for the P3HT/$PC_{61}BM$ cell (3.79 mA/cm^2), revealing that **4** showed weaker interaction with $PC_{61}BM$ than P3HT.[41] Pyrene-cored donor **4** showed the weaker interaction with $PC_{61}BM$. The high V_{oc} values above 1.0 V might be cased by a small recombination loss of carriers in active layer due to the weak intermolecular interactions between the disk-shaped donor and the fullerene acceptor.

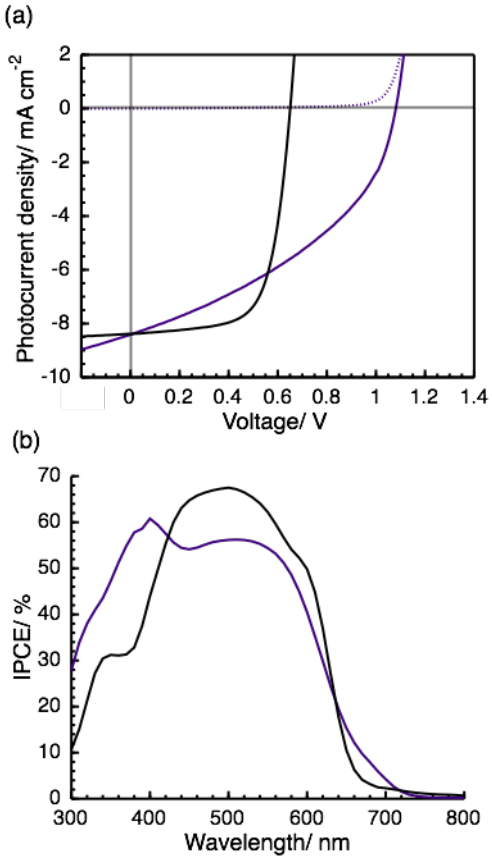

Figure 4. (a) Photocurrent voltage curve obtained with BHJ solar cells based on **4**/

$PC_{71}BM$ (purple) and P3HT/ $PC_{61}BM$ (black) blended active layers under a standard global AM 1.5 solar condition (solid line) and dark current (dotted line). b) Incident photon-to-current conversion efficiency spectrum based on **4**/$PC_{71}BM$ (purple) and P3HT/$PC_{61}BM$ (black) blended active layers.

Figure 4 shows the *J-V* and incident-photon to current conversion efficiency (IPCE) characteristics of a **4**/$PC_{71}BM$ device (**4**:$PC_{71}BM$ composition ratio = 1:3 w/w). Since $PC_{71}BM$ has a higher absorption coefficient in the visible range, the J_{sc} value was improved significantly by changing from $PC_{61}BM$ to $PC_{71}BM$. The **4**/$PC_{71}BM$ cell showed a PCE of 3.7 % with a J_{sc} of 8.4 mA/cm^2, V_{oc} of 1.09 V, and *FF* of 41% under one sun condition and exhibited a broad IPCE between 300 and 700nm with a maximum of 57 % at 530 nm (Figure 4b). The IPCE spectra followed the absorption feature of rhodanine-terminated pyrene-cored donor **4** and $PC_{71}BM$. The low *FF* value of the **4**/$PC_{71}BM$ cell suggests a poor balance of charge carrier mobilities in the active layer. Further enhancement of solar cell performance requires the improvement of hole mobility in the stacking of pyrene-cored donors. Investigations are underway to optimize the structure of pyrene-cored donors to improve the PCEs in BHJ solar cells.

Conclusion

Four disk-shaped donors **1-4** comprised of a pyrene core and dithiophene linkers, and rhodanine terminal units were synthesized as the donor components of solution-processed BHJ solar cells. The introduction of rhodanine terminal units resulted in expansion of light-harvesting area in the visible light region as well as enhancement of molar absorption coefficients compared to the pyrene-cored donors

lacking rhodanine terminal units. The length of peripheral alkyl chains changed molecular ordering and carrier transport properties in solid state. The HOMO and LUMO energy levels of these materials were suitable for the donor component in BHJ solar cells with fullerene acceptor. The BHJ solar cells were fabricated by the solution process using mixed solutions of pyrene-cored donors with fullerene acceptors. The PCE values strongly depended on the structure of the donor. In addition, the shortening of the peripheral alkyl chain length in the dithiophene linkers improved the PCE due to its better hole-mobility in the film. The highest PCE of BHJ solar cells achieved a **4**/ $PC_{71}BM$ device with a PCE of 3.7%, J_{sc} of 8.4 mA/cm^2, V_{oc} of 1.09 V, and *FF* of 41% under one sun condition.

Experimental Section

General. NMR spectra were recorded on a Bruker AVANCE 400 FT NMR spectrometer at 400.13 MHz and 100.61MHz for ^{1}H and ^{13}C in $CDCl_3$ solution. Chemical shifts are reported relative to internal TMS. UV-Vis spectra were measured on a JASCO V-650. MALDI-TOF mass spectra were obtained on a Bruker autoflex with dithranol as matrix. The transition temperatures were measured by differential scanning calorimetry with a SII DSC 6200 operated at a scanning rate of 10^{o}C min^{-1} on heating and cooling. The apparatus was calibrated with indium as standard. The XRD patterns were obtained with a Rigaku XRD-DSC with Cu Kα radiation. Atomic force microscopy images were acquired in tapping mode by a JEOL JSPM-5400 system. The samples for AFM were prepared by the spin-coating of $CHCl_3$ solutions on quartz substrate. Cyclic voltammetric measurements were recorded on an ALS 700 potentiostat using a three cell electrode system with a Pt working electrode, a Pt counter electrode and an Ag/AgCl reference electrode. $TBAPF_6$ was used as the electrolyte.

Materials. All chemicals were purchased from commercial suppliers and used without purification. P3HT was purchase from Rieke Metals Inc. (electronic grade) and used without any purification. 1,3,6,8-Tetrabromopyrene and

5-bromo-3-hexylthiophene-2-carbaldehyde were synthesized according to the literature methods.[24,42,43] Column chromatography was performed with silica gel (Wakogel C-200). Recycling preparative gel permeation chromatography was carried out by a JAI recycling preparative HPLC using $CHCl_3$ as an eluent. Analytical thin layer chromatography was performed with commercial Merck plates coated with silica gel 60 F_{254}. The purities of target compounds were confirmed by NMR, MALDI-TOF-Ms and analytical HPLC.

Four pyrene-cored donors **1-4** were prepared according to the synthetic route as shown in Scheme 1.

1: **8** (48mg, 0.05mmol) was dissolved in solution of dry $CHCl_3$ (15ml), then a few drops of dry piperidine and 3-ethylrhodanine (0.1g, 0.62mmol) was added. The mixture was stirred at 65˚C for 24h. After cooling to room temperature, the reaction mixture was poured into water, extracted with $CHCl_3$. The organic layer was dried over magnesium sulfate and the solvent was evaporated. The residue was purified by column chromatography on silica gel by eluting with $CHCl_3$ and recycling preparative HPLC to give **1** as dark purple solid (37mg, yield 59 %). ^{1}H-NMR (400.13MHz, $CDCl_3$): δ (ppm) =8.37 (s, 4H, Ar*H*), 8.09 (s, 4H, Ar*H*), 7.97 (s, 2H, Ar*H*), 7.50 (s, 2H, Ar*H*), 7.18 (s, 2H, Ar*H*), 4.22 (q, *J*=6.7Hz, 4H, -CH_2-), 2.93 (t, *J*=7.9Hz, 4H, -CH_2-), 2.84 (t, *J*=7.9Hz, 4H, -CH_2-), 1.85-1.71 (m, 4H, -CH_2-), 1.79-1.72 (m, 4H, -CH_2-), 1.41-1.34 (m, 24H, -CH_2-), 1.32 (t, *J*=6.8Hz, 6H, -CH_3), 0.96-0.90 (m, 12H, -CH_3). MALDI-TOF-Ms: *m/z*=1207.97 (M+H); Calculated for $C_{68}H_{76}N_2O_2S_8$: *m/z*=1208.37. UV-Vis ($CHCl_3$): λ_{max} (log ε) = 510 (4.82), 345 (4.75), 327 (4.64).

2: Yield 66%. ^{1}H-NMR (400.13MHz, $CDCl_3$): δ (ppm) = 8.52 (d, J=9.2Hz, 2H, Ar*H*), 8.24 (s, 2H, Ar*H*), 8.17 (s, 1H, Ar*H*), 8.09 (d, *J*=9.2Hz, 2H, Ar*H*), 7.90 (s, 1H, Ar*H*), 7.27 (s, 2H, Ar*H*), 7.14 (s, 2H, Ar*H*), 4.18 (q, *J*=6.7Hz, 4H, -CH_2-), 2.92 (t, *J*=7.6Hz, 4H, -CH_2-), 2.76 (t, *J*=7.6Hz, 4H, -CH_2-), 1.83-1.75 (m, 4H, -CH_2-), 1.70-1.62 (m, 4H, -CH_2-), 1.60 (s, 9H, -CH_3), 1.51-1.48 (m, 4H, -CH_2-), 1.41-1.32 (m, 20H, -CH_3), 1.30 (t, *J*=6.8Hz, 6H, -CH_2-), 0.95-0.88 (m, 12H, -CH_2-). ^{13}C-NMR ($CDCl_3$, 100.61Hz): δ (ppm) =192.6, 167.9, 151.1, 150.2, 156.0, 143.6, 142.5, 142.1, 132.3, 131.5, 130.0, 129.3, 128.8, 128.7, 126.1, 124.9, 123.9, 123.5, 119.5, 40.3, 35.7, 32.3, 32.3, 32.0, 31.5, 31.0, 30.5, 29.8, 29.5, 29.4, 23.2, 23.0, 21.7, 14.6, 14.5. MALDI-TOF-Ms: *m/z*=1264.06 (M+H); Calculated for $C_{72}H_{84}N_2O_2S_8$: *m/z*=1264.43. UV-Vis ($CHCl_3$): λ_{max} (log ε) = 494 (4.95), 395 (4.55), 314 (4.67).

3: Yield 65 %. ^{1}H-NMR (400.13MHz, $CDCl_3$): δ (ppm) = 8.37 (s, 4H, Ar*H*), 8.10 (s, 2H, Ar*H*), 7.88 (s, 4H, Ar*H*), 7.20 (s, 4H, Ar*H*), 7.16 (s, 4H, Ar*H*), 4.22 (q, *J*=6.7Hz, 8H, -C*H*$_2$-), 2.93 (t, *J*=7.6Hz, 8H, -C*H*$_2$-), 2.82 (t, *J*=7.6Hz, 8H, -C*H*$_2$-), 1.82-1.74 (m, 8H, -C*H*$_2$-), 1.73-1.68 (m, 8H, -C*H*$_2$-), 1.54-1.37 (m, 48H, -C*H*$_2$-), 1.33 (t, *J*=7.2Hz, 12H, -C*H*$_3$), 0.97-0.91 (m, 24H, -C*H*$_3$). ^{13}C-NMR ($CDCl_3$, 100.61Hz): δ (ppm) =192.0, 167.4, 150.6, 142.0, 141.2, 132.2, 131.9, 131.7, 129.2, 123.2, 119.1, 40.0, 31.8, 31.7, 31.2, 30.4, 29.5, 29.2, 29.1, 22.8, 14.2. MALDI-TOF-Ms: *m/z*=2214.38 (M+H); Calculated for $C_{120}H_{142}N_4O_4S_{16}$: *m/z*=2214.67. UV-Vis ($CHCl_3$): λ_{max} (log ε) = 501 (5.18), 320 (4.84).

4: Yield 79%. ^{1}H-NMR (400.13MHz, $CDCl_3$): δ (ppm) = 8.18 (s, 4H, Ar*H*), 7.97 (s, 2H, Ar*H*), 7.81 (s, 4H, Ar*H*), 7.12 (s, 4H, Ar*H*), 7.10 (s, 4H, Ar*H*), 4.22 (q, *J*=6.7Hz, 8H, -C*H*$_2$-), 2.90 (t, *J* = 7.6Hz, 8H, -C*H*$_2$-), 2.47 (s, 12H, -C*H*$_2$-), 1.81-1.73 (m, 8H, -C*H*$_2$-), 1.55-1.51 (m, 8H, -C*H*$_2$-), 1.44-1.41 (m, 16H, -C*H*$_2$-), 1.33 (t, *J*=7.2Hz, 12H, -C*H*$_3$), 0.97 (t, *J*=7.2Hz, 12H, -C*H*$_3$). ^{13}C-NMR ($CDCl_3$, 100.61Hz): δ (ppm) =191.8, 167.3, 145.0, 143.3, 141.9, 141.2, 132.1, 131.7, 130.7, 128.9, 128.2 127.8, 125.0, 124.9, 124.5, 123.0, 118.8, 45.6, 45.2, 40.1, 37.5, 37.1, 34.5, 33.4, 32.8, 31.8, 32.5, 30.5, 30.2, 30.1, 29.7, 29.6, 27.5, 27.1, 22.9, 20.4, 19.8, 14.8, 14.3. MALDI-TOF-Ms: *m/z*=1934.07 (M+H); Calculated for $C_{100}H_{102}N_4O_4S_{16}$ *m/z*=1934.34. UV-Vis ($CHCl_3$): λ_{max} (log ε) = 502 (5.16), 321 (4.78).

Fabrication of BHJ Solar Cells: Indium tin oxide (ITO) patterned glass substrates were cleaning with sonication in neutral detergent, distilled water, acetone and 2-propanol. The substrates were dried and apply UV-O_3 treatment for 30min. Electron blocking layer were prepared by spin-coated the PEDOT:PSS (H. C. Starck) with a thickness of 40 nm. The substrates were baked at 200˚C for 30 min. A solution containing a mixture of pyrene-cored donors and fullerene derivatives in chloroform were spin-coated onto the PEDOT: PSS layer, and apply thermal annealing treatment at 150˚C for 10min in the argon filled globe box. Titanium oxide solution was spin-coated onto the active layer then place in air for 30min. The counter electrode of aluminum was prepared by thermal deposition with a thickness of 100nm. Current density-voltage (*J-V*) characteristics were measured using a Keithley 2400 Source Measure Unit. Performance of BHJ solar cells devices was measured under one-sun conditions (AM 1.5, 100mW/cm^2) by a solar simulator (XES-151S, Sanei electric Inc.).

Acknowledgment. We acknowledge financial support from the New Energy and Industrial Technology Development Organization (NEDO) of Japan.

Electronic Supplementary Information (ESI) available. [Synthetic procedures of 6-18, ^{1}H NMR spectra of 1-4, TGA, DSC, XRD, AFM images, hole mobility measurements and solar cell performance]. See DOI: 10.1039/c000000x/

References

1. S. Günes, H. Neugebauer, N. S. Sariciftci, *Chem. Rev.*, 2007, **107**, 1324.
2. A. J. Heeger, *Adv. Mater.*, 2014, **26**, 10.
3. M. T. Dang, L. Hirsch, G. Wantz, J. D. Wuest, *Chem. Rev.*, 2013, **113**, 3734.
4. Y. Huang, E. J. Kramer, A. J. Heeger, G. C. Bazan, *Chem. Rev.*, 2014, **114**, 7006.
5. T. M. Clarke, J. R. Durrant, *Chem. Rev.*, 2010, **110**, 6736.
6. Y. –J. Cheng, S. –H. Yang, C. –S. Hsu, *Chem. Rev.*, 2009, **109**, 5868.
7. M. Riede, T. Mueller, W. Tress, R. Schueppei, K. Leo, *Nanotechnology*, 2008, **19**, 424001.
8. J. Roncali, *Acc. Chem. Res.*, 2009, **42**, 1719.
9. B. Walker, C. Kim, T. –Q. Nguyen, *Chem. Mater.*, 2011, **23**, 470.
10. A. Mishra, P. Bäuerle, *Angew. Chem. Int. Ed.*, 2012, **51**, 2020.
11. B. Walker, A. B. Tamayo, X. –D. Dang, P. Zalar, J. H. Seo, A. Garcia, M. Tantiwiwat, T. –Q. Nguyen, *Adv. Funct. Mater.*, 2009, **19**, 3063.
12. Y. Matsuo, Y. Sato, T. Niinomi, I. Soga, H. Tanaka, E. Nakamura, *J. Am. Chem. Soc.*, 2009, **131**, 16048.
13. G. Wei, S. Wang, K. Renshaw, M. E. Thompson, S. R. Forrest, *ACS Nano*, 2010, **4**, 1927.
14. G. Wei, S. Wang, K. Sun, M. E. Thompson, S. R. Forrest, *Adv. Energy Mater.*, 2011, **1**, 184.
15. H. Shang, H. Fan, Y. Liu, W. Hu, Y. Li, X. Zhan, *Adv. Mater.*, 2011, **23**, 1554.
16. S. Loser, C. J. Bruns, H. Miyauchi, R. P. Prtiz, A. Facchetti, S. I. Stupp, T. J. Marks, *J. Am. Chem. Soc.*, 2011, **133**, 8142.
17. J. Zhang, D. Deng, C. He, Y. He, M. Zhang, Z. –G. Zhang, Z. Zhang, Y. Li, *Chem. Mater.*, 2011, **23**, 817.
18. Y. Sun, G. C. Welch, W. L. Leong, C. J. Takacs, G. C. Bazan, A. J. Heeger, *Nat.*

Mater., 2012, **11**, 44.

19. T. S. van der Poll, J. A. Love, T. –Q. Nguyen, G. C. Bazan, *Adv. Mater.*, 2012, **24**, 3646.
20. J. Zhou, X. Wan, Y. Liu, Y. Zuo, Z. Li, G. He, G. Ling, W. Ni, C. Li, X. Su, Y. Chen, *J. Am. Chem. Soc.*, 2012, **134**, 16345.
21. J. Zhou, Y. Zuo, X. Wan, G. Long, Q. Zhang, W. Ni, Y. Liu, Z. Li, G. He, C. Li, B. Kan, M. Li, Y. Chen, *J. Am. Chem. Soc.*, 2013, **135**, 8484.
22. K. Takemoto, M. Karasawa, M. Kimura, *ACS Appl. Mater. Interfaces*, 2012, **4**, 6289.
23. T. M. Figueira-Duarte, K. Müllen, *Chem. Rev.*, 2011, **111**, 7260.
24. M. Uchimura, Y. Watanabe, F. Araoka, J. Watanabe, H. Takezoe, G. Konishi, *Adv. Mater.*, 2010, **22**, 4473.
25. Y. Niko, S. Kawauchi, S. Otsu, K. Tokumaru, G. Konishi, *J. Org. Chem.*, 2013, **78**, 3196.
26. Y. Li, Q. Gao, Z. Li, J. Pei, W. Tian, *Energy Environ. Sci.*, 2010, **3**, 1427.
27. P. –L. T. Boudreault, A. Najari, M. Leclerc, *Chem. Mater.*, 2011, **23**, 456.
28. Z. Li, G. He, X. Wan, Y. Liu, J. Zhou, G. Lomng, Y. Zuo, M. Zhang, Y. Chen, *Adv. Energy Mater.*, 2012, **2**, 74.
29. K. Colladet, S. Fourier, T. J. Cleij, L. Lutsen, J. Gelan, D. Vanderzande, L. H. Nguyen, H. Neugebauer, S. Sariciftci, A. Aguirre, G. Janssen, E. Goovaerts, *Macromolecules*, 2007, **40**, 65.
30. R. Grisorio, G. Allegretta, G. P. Suranna, P. Mastrorilli, A. Loiudice, A. Rizzo, M. Mazzeo, G. Gigli, *J. Mater. Chem.*, 2012, **22**, 19752.
31. A. R. Murphy, P. C. Chang, P. VanDyke, J. Liu, J. M. Fréchet, V. Subramanian, D. M. DeLongchamp, S. Sambasivan, D. A. Fischer, E. K. Lin, *Chem. Mater*., 2005, **17**, 6033.
32. S. Samitsu, T. Shimomura, S. Heike, T. Hashizume, K. Ito, *Macromolecules*, 2008, **41**, 8000.
33. J. D. Dunitz, A. Gavezzotti, *Chem. Soc. Rev.*, 2009, **38**, 2622.
34. G. G. Malliaras, J. R. Salem, P. J. Brock, C. Scott, *Phys. Rev. B*, 1998, **58**, R13411.
35. C. Goh, R. J. Kline, M. D. McGehee, E. N. Kadnikova, J. M. J. Fréchet, *Appl. Phys. Lett.*, 2005, **86**, 12110.
36. Y. Liang, D. Feng, Y. Wu, S. –T. Tsai, G. Li, C. Ray, L. Yu, *J. Am. Chem. Soc.*,

2009, **131**, 7792.

37. Z. B. Wang, M. G. Helander, M. T. Greiner, J. Qiu, Z. H. Lu, *J. Appl. Phys.*, 2010, **107**, 034506.
38. M. D. Perez, C. Borek, S. R. Forrest, M. E. Thompson, *J. Am. Chem. Soc.*, 2009, **131**, 9281.
39. K. Vandewal, K. Tvingstedt, A. Gadisa, O. Inganäs, J. Manca, *Nat. Mater.*, 2009, **8**, 904.
40. L. Yang, H. Zhou, W. You, *J. Phys. Chem. C*, 2010, **114**, 16793.
41. G. Long, X. Wan, B. Kan, Y. Liu, G. He, Z. Li, Y. Zhang, Y. Zhang, M. Zhang, Y. Chen, *Adv. Energy Mater.*, 2013, **3**, 639.
42. K. C. Stylianou, R. Heck, S. Y. Chong, J. Bacsa, J. T. A. Jones, Y. Z. Khimyak, D. Bradshow, M. J. Rosseinsky, *J. Am. Chem. Soc.*, 2010, **132**, 4119.
43. Y. Wang, L. Xu, X. Wei, X. Li, H. Ågren, W. Wua and Y. Xie, *New J. Chem.*, 2014, **38**, 3227.